Available online at www.sciencedirect.com
SCIENCE DIRECT®

Journal of the European Ceramic Society 24 (2004) 661–668

www.elsevier.com/locate/jeurceramsoc

Ceramic TiO_2-foams: characterisation of a potential scaffold

Håvard Haugen*, Julia Will, Anne Köhler, Ursula Hopfner, Joachim Aigner, Erich Wintermantel

Central Institute for Medical Engineering, Technische Universität München, Boltzmannstrasse 11, D-85748 Garching, Germany

Received 19 December 2002; received in revised form 12 March 2003; accepted 6 April 2003

Abstract

The Schwartzwalder process was chosen for the production of ceramic TiO_2 scaffolds and showed a fully open structure with a permeability for water of 39%. The window sizes were 445 μm (45 ppi foams) and 380 μm for the 60 ppi foams. The porosity of all foams was above 78% ($n=8$). It was shown that scaffolds can be produced with defined pore sizes, shape and architecture, which is a requirement for scaffold production. The macro- and microarchitecture was reproducible. Hence a reproducible ceramic scaffold processing method has been established. The interconnectivity of the pores in the scaffold was tested with a novel method. For the tests a new device was constructed where the permeability was linked to the degree of interconnectivity. Results from the permeability measurements in the mercury intrusion meter and permeability tester show that increasing pore size increases the rate of permeability. The tortuosity, which was measured in the mercury intrusion meter, was several factors higher for 60 ppi foams compared to 45 ppi and therefore also understates the lower permeability. An initial cell culture test showed that fibroblasts adhere on the foam's surface.

Keywords: Foams; TiO_2; Biomedical application; Porosity

1. Introduction

In the United States one quarter of patients in need of organ transplantation die while waiting for a suitable donor. Studies have shown that this gap will continue to widen in the future.[1] One principle of tissue engineering is to harvest cells, expand the cell population in vitro, if necessary, and seed them onto a supporting three-dimensional scaffold, where the cells grow into a complete tissue or organ.[33] For most clinical applications, the choice of scaffold material and structure is crucial.[15]

In order to achieve a high cell density within the scaffold, the material has to have a high surface area to volume ratio. The pores must be open and large enough so that the cells can migrate into the scaffolds. When cells have attached to the material surface there must be enough space and channels to allow for nutrient delivery, waste removal, exclusion of material or cells and protein transport, which is only obtainable with an interconnected network of pores.[23] Biological responses to implanted scaffolds are also influenced by scaffold design factor such as three-dimensional microarchitecture.[3,35] In addition to the structural properties of the material, physical properties of the material surface for cell attachment are essential.

One of the most promising biocompatible materials in this sense has been proven in previous studies to be a bioactive ceramic, TiO_2.[10,20,21,37] This material has shown particular biocompatible properties, where scaffolds were implanted in rats for 55 weeks without any signs of inflammatory responses or encapsuling.[36]

Little work has been made in the three-dimensional open pore manufacturing of titanium dioxide.[24,25] The objective of this work was to produce ceramic foams with their defined macro-, micro- and nano-structures and to show the possible application of ceramic foams as scaffolds for cell cultures.

1.1. Scaffolds properties

The major requirement of any proposed scaffold processing method is not only the utilization of the biocompatible materials. The technique should also allow

* Corresponding author.

0955-2219/03/$ - see front matter © 2003 Elsevier Ltd. All rights reserved.
doi:10.1016/S0955-2219(03)00255-3

for a controlled material structure such as pore size and porosity, which are important factors in organ regeneration. A highly porous scaffold is necessary to allow cell seeding or migration throughout the material. Pore size plays a critical role in both tissue in growth and the internal surface area available for cell attachment. These parameters are dependent on the cell type to be seeded.[29] In order to achieve high cell attachment within the scaffold, the material has to have a high internal surface area to volume ratio.[9,34] This ratio can be increased producing material with small-sized pores.

In order to allow cells to migrate into the scaffold, its pores have to be open and interconnective. The mass transport of nutrients and waste from the cell culture inside of the scaffold is also dependent on this factor. The interconnectivity of the pores in the manufactured scaffolds was measured by permeability.

1.2. Ceramic foams

Highly porous ceramics can be found in numerous technical fields due to their chemical inertness. Most chemical applications for ceramic foams involve either filtration or separation. Other application of porous ceramics are known in thermal protection, gas combustion burners, catalysis, filtration of hot gas streams and molten metals which is the most important use of open-pore ceramic foams.[4,18,32] Porous ceramic foams are commonly classified into two types: closed-pore foams and open-pore (or reticulated) foams. The closed-pore foams have structures resembling a network of soap bubbles. The open-pore foams are identical to the closed cell ones except the membranes have been removed which produces large channels of interconnected cells, the main advantage of which is its "flow-through" capability. Liquids and gases can flow through the structure with minimal resistance. Ceramic foams can be produced in many configurations and pore sizes by using a variety of different processes.[17,18,27] For the fabrication of TiO_2 scaffold the "polymer sponge method" was chosen.[28]

1.3. Polymer sponge method

Reticulated open-pore ceramics are produced via the replication of a polymeric porous structure. The patent on this technique called the "replication" or "polymer-sponge" method was first filed by Schwartzwalder and Somers in 1963.[28] It is the standard method for producing alumina, zirconium, silicon carbide and other ceramic foams.[6,14,22,26,27]

The foams are manufactured by coating a polyurethane foam with a ceramic slurry. The polymer, having already the desired macrostructure, simply serves as a sacrificial scaffold for the ceramic coating. The slurry infiltrates the structure and adheres to the surface of the polymer. Excess slurry is squeezed out leaving a ceramic coating on the foam struts. After drying, the polymer is slowly burned away in order to minimize damage to the porous coating. Once the polymer has been removed, the ceramic is sintered to the desired density. The process replicates the macrostructure of the polymer, and results in a rather distinctive microstructure within the struts. A flowchart of the process is given in (Fig. 1).

The pore size of the polymer foams is classified in terms of pores per linear inch: ppi. In this study foams with ppi numbers of 45 and 60 ppi were chosen to obtain pore diameters which needed for cell culture. Foams with other ppi-numbers are commercially available.

The most important property governing the behavior of ceramic foams is the relative density,[6] i.e. the density of the bulk foam normalized by the theoretical density of the solid which forms the cell edges and faces.

2. Experimental

2.1. Polymer foams

Examples of the used polymer precursors are illustrated (Fig. 2). Fully reticulated polyester based polyurethane foams with ppi numbers of 45 and 60 ppi (Bulbren S, Eurofoam GmbH, Wiesbaden, Germany) were used in this study. The foams were supplied in large plates 5 mm in thickness and were cut to size by punching them out with a metal stamp to cylinders of 10 mm in diameter. The single struts are characterized by

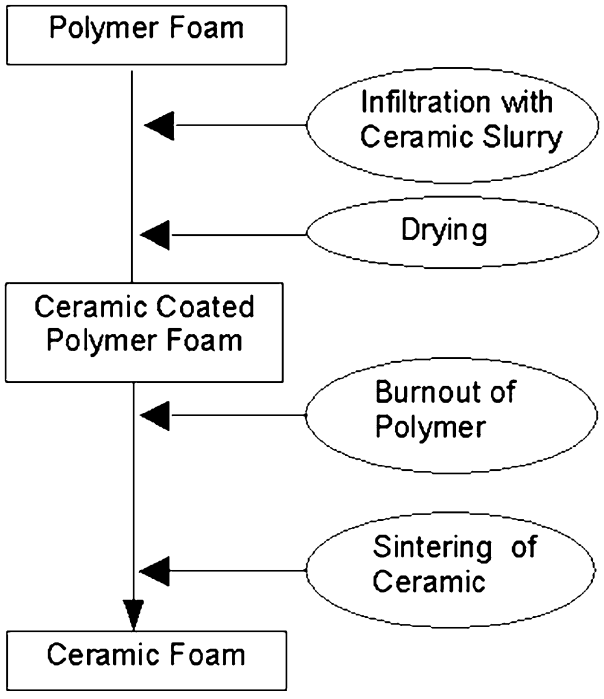

Fig. 1. Flowchart of the polymer sponge method.

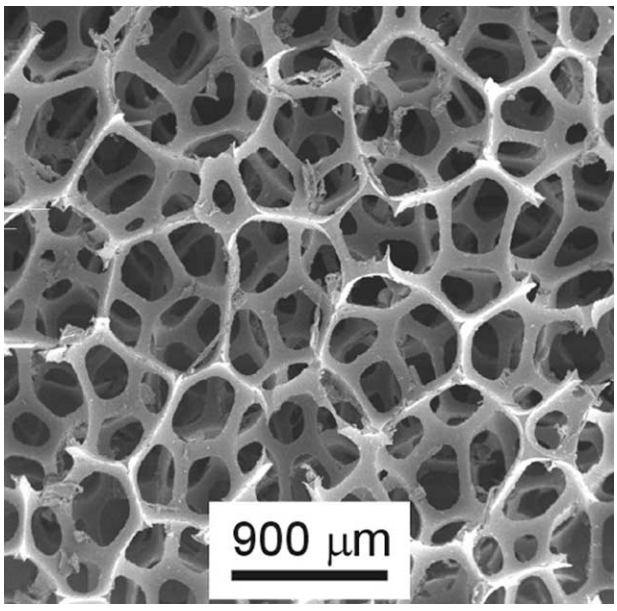

Fig. 2. Polyester based polyurethane foams 45 ppi.

the diameter of a triangle as illustrated (Fig. 3) where also some residue on the polymer struts can be seen. These remains are from the reticulation process by a gas explosion.

2.2. Scaffold fabrication

The suspension for the impregnation of the polymers is prepared using the following recipe: 88.4 g of TiO_2 powder (Kronos TiO_2 No 1171, Kronos Titan GmbH, Leverkusen, Germany) with a median grain size of 0.3 μm mixed with 25.8 g deionised water. After a milling time of an hour in a ball milling additional powder was given into the suspension in several steps up to a volume content of 57 vol.% (133.4 g). 0.13 g Polysaccharide binder (Product KB 1013, Zschimmer & Schwarz GmbH, Lahnstein, Germany) was added and the homogenisation in the ball milling time was 10 min.

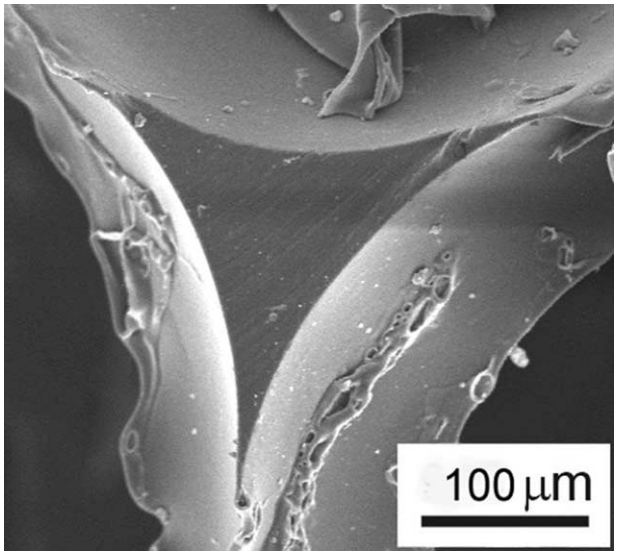

Fig. 3. SEM picture, single strut of a polyurethane foam. The remains from the reticulation process can be viewed on the surface.

The polymer foams were then dipped into the ceramic slurry, which then later were squeezed with the help of a handroll, leaving only a thin layer of slurry on the polymer scaffold. The samples were then placed onto a porous ceramic plate and dried at room temperature for at least 18 h. The heating schedule for the burnout of the polymer and the sintering of the ceramic part was chosen as follows: slowly heating to 450 °C with 0.5 K/min, 1 h holding time at 450 °C, heating to 1150 °C with 3 K/min, cooling to room temperature with 5 K/min. Simultaneous Thermal Analysis (STA) (Jupiter, Netzsch Gerätebau, Selb, Germany) measurements (Fig. 4) shows the burn-out temperature and removal of the polymer substrate. The STA combines the DSC (Differential Scanning Calorimeter) and TG (Thermal Gravity) signals.

2.3. Characterization

2.3.1. Pore size distribution and porosity

The pore size distributions were measured by mercury intrusion porosimetry (Autopore IV, Micromeretics, Norcoss, GA, USA). A solid penetrometer with 6 ml bulb volume (model 07-044506-01, Micromeritics, Norcoss, GA, USA) was used. The intrusion chamber was then filled with mercury at a pressure of 3.45 kPa and the samples were penetrated with mercury until a maximum pressure of 420 MPa at which the total intrusion volume reached a plateau. The pore diameter distribution was obtained using the Washburn equation:

$$D = \frac{-4\gamma\cos\theta}{P} \quad (1)$$

where D is the pore diameter, λ is the surface tension of mercury (480 dyne cm^{-1}), θ is the contact angle between

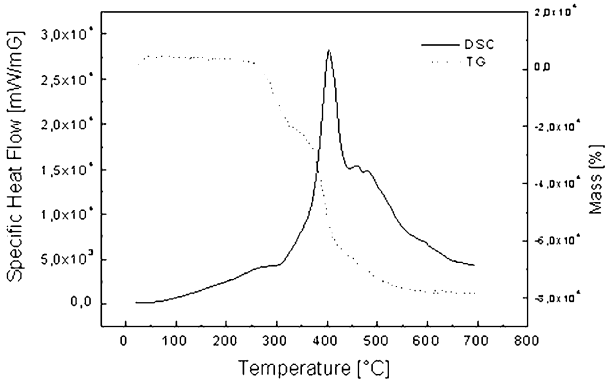

Fig. 4. STA measurement of burn-out temperature of polymer scaffold from TiO_2 scaffold (Abbreviations: DSC = Differential Scanning Calorimeter, TG = Thermal Gravity).

mercury and TiO_2, which was taken to be 141° and P is the pressure measured during the mercury intrusion process. The mean pore diameter of the sample was calculated from the measured pore diameter distribution, and the porosity was obtained from the total intruded volume.

2.4. Micro- and macrostructure analysis

The scaffolds were sputter coated with gold (Cool Sputter, Bal-Tec AG, Balzers, Liechtenstein) for 40 s at current of 40 mA before examination in a Scanning Electron Microscope (SEM) (Hitachi S-3500-N, Hitachi High Technologies, Japan) under high vacuum with current range between 5 and 15 kV.

2.5. Permeability

As previously described the macroscopic foams structure must have interconnective channels to allow for nutrient delivery, waste removal, exclusion of material or cells and protein transport.[23]

The permeability was measured with a self-constructed permeability-meter. Water was used as flow media. The sample was located in fitting consisting of two half shells. The fitting had a round opening with a diameter of 5 mm and was screwed on the aluminum pipe. The sample has to bear a water pressure resulting from the high of the water column (1 m). The percolation rate was measured with a zero flow rate with no sample set as 100%. Fifteen samples were tested 10 times each.

In order to validate the experimental results described above, four sample were tested for permeability using the mercury intrusion porosimetry. Katz and Thompson have used the percolation theory applied to laminar flow in porous media to develop a mercury porosimetry-based prediction for the ratio of the fluid permeability k to the electrical conductivity σ of a porous material.[12] Their main result is the prediction that

$$\frac{k}{\sigma} = \frac{cd_c^2}{\sigma_o} \tag{2}$$

where σ_o is the electrical conductivity of the pore-saturating fluid, c is a calculated constant on the order of 0.01 that depends weakly on the assumptions made for the relationship between pore length and pore diameter[2] and d_c is the threshold pore diameter as measured by mercury porosimetry.[5]

The electrical conductivities of the tested samples were unknown and had to be calculated from obtained mercury intrusion porosimetry data. Firstly, the characteristic length, L_{char}, must be determined and was found from the threshold pressure, P_{thres}, using the Washburn equation (see Eq. (1)). The threshold pressure is the pressure at which the intrusion volume versus pressure curve is steepest, which was calculated by supplied product software. L_{char} is defined in the following way. If the pore space is sequentially built up starting with the largest pores working down, then L_{char} is the diameter of the pore that just completes the first continuous pathway through the material. This pathway consists only of the pores with L greater than or equal to L_{char}.[5] Katz and Thompson found experimentally that L_{char} correspond closely to the inflection point on the cumulative intrusion curve.[11]

The conductivity for the TiO_2 samples were calculated using the length at which conductance is maximum, L_{max}. The conductance is maximum when $(I–I_{thresh})D^3$ is maximum, where I is the intrusion volume and D is the diameter of the pore.

The specific volume intruded at pores larger than L_{char}, I_{thresh}, is also used, and was calculated by interpolating the specific intrusion volume versus pore diameter curve at L_{char}. The fractional volume of connected pore space involving pore widths of size L_{max} and larger, S_{Lmax}, can be calculated by interpolating the specific intrusion volume versus pores size curve to L_{max} and dividing by the total specific intrusion volume I_{tot}. Hence, the absolute permeability k can rewritten from Eq. (2) and be calculated as follows:[12]

$$k = \frac{1}{89} L_{max}^2 \cdot \frac{L_{max}}{L_{char}} \cdot I_{tot} \cdot Y_b \cdot S_{Lmax} \tag{3}$$

where Y_b = sample weight/bulk volume

2.6. Cell adhesion test

After the sterilization in an autoclave the foams ($n = 2$) were seeded with the 3T3 fibroblastic cell line (American Type Culture Collection, Manassas VA, USA) and cultured in Dulbecco's Modified Eagle Medium DMEM (Biochrom AG, Berlin, Germany) with 10% Fetal Calf Serum FCS (Biochrom AG, Berlin, Germany) at 37 °C and 5% CO_2-atmosphere. First, the sterilized foams were moistened with culture medium and then placed in 48-well-plates (Corning Lifesciences, Wiesbaden, Germany).

The cells were then seeded at a concentration of 5×10^4 and 5×10^5 in a volume of 100 μl culture medium directly on the scaffolds. After a sedimentation-time of 30 min at 37 °C and 5% CO_2-atmosphere, the wells were filled with 800 μl culture medium and subsequently cultured (37 °C and 5% CO_2). The scaffolds were washed twice with Phosphate Buffered Solution PBS (Biochrom AG, Berlin, Germany) 7 days after seeding and fixed 2 days at 4 °C with 3% glutaraldehyde (Merck, Darmstadt, Germany) in PBS (Biochrom AG, Berlin, Germany).

The samples were then dehydrated using a graded ethanol (Merck, Darmstadt, Germany) series from 10 to 100%, with three times 10-min incubation at each step.

Dehydration was then completed by critical point drying using CO_2 (CPD-030, Bal-Tec AG, Balzers, Liechtenstein) The scaffolds were sputtered and examined in a scanning electron microscope according to procedure previously described.

3. Results

3.1. Foam structure

The macrostructure of the sintered foams are characterized by a fully open structure for both ppi-numbers (Fig. 5), although a very low number of closed cells are always present. Three types of porosity can be distinguished: a fine-scale porosity within the ceramic part (Fig. 6), a triangular pore in the centre of the struts (Fig. 7) and large pores which are also called "windows" (Fig. 8).

3.2. Pore size distribution and porosity

The pore size distribution of 45 and 60 ppi foams (Fig. 9) can be described with three regions: (1) a fine-scale portion within the solid portion, 0.5–1.7 μm for the 45 ppi foams and 0.5–1.2 μm for the 60 ppi foams; (2) pores resulting from the pyrolysis of the polymer struts with pore sizes from 12–45 μm with a maximum pore size at 0.15 μm (45 ppi) and 7–25 μm with a maximum pore size at 19 μm (60 ppi). These pores are in the

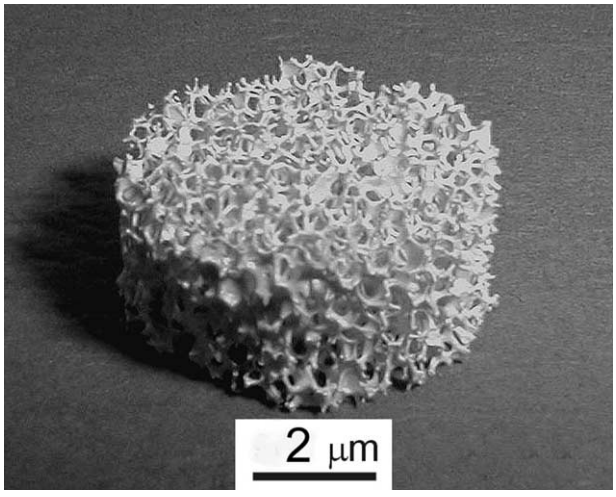

Fig. 5. Macrostructure of a sintered 60 ppi TiO2-foam.

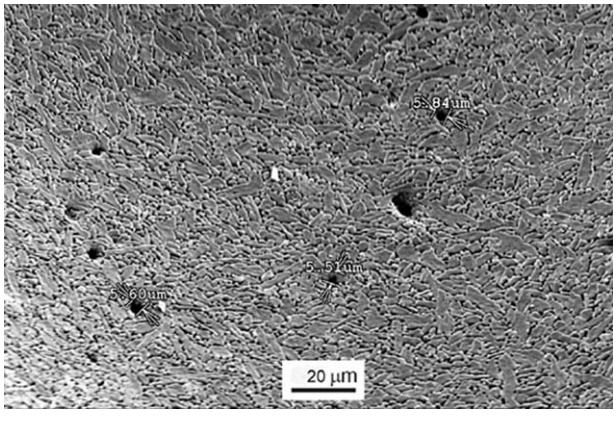

Fig. 6. SEM picture showing fine-scale porosity within the ceramic grain.

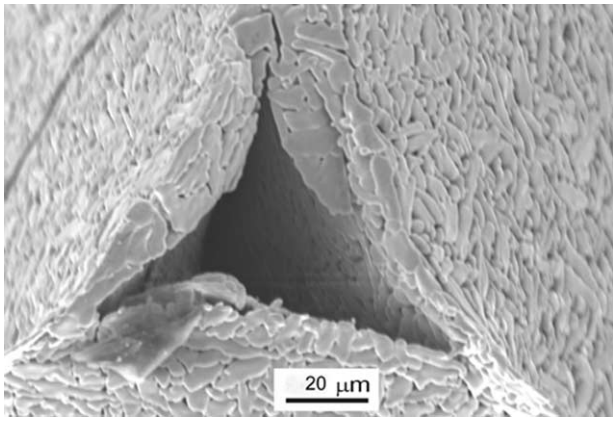

Fig. 7. SEM picture with a triangular void resulting from the pyrolysis of the polymer.

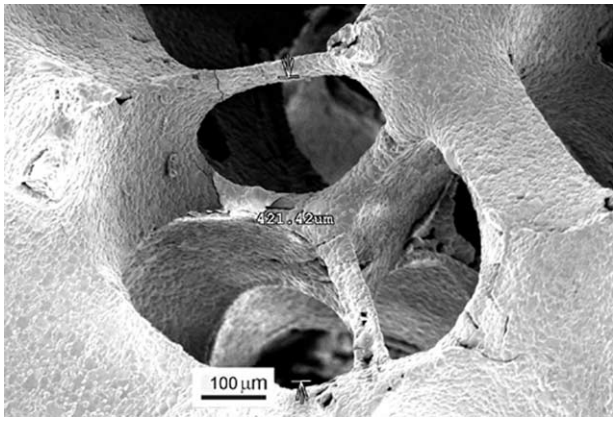

Fig. 8. SEM picture of sintered 45 ppi TiO_2 foams with a pore window size of 420 μm.

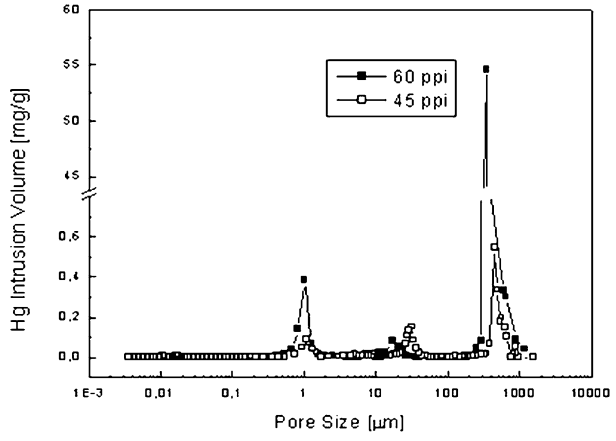

Fig. 9. Pore size distribution from mercury intrusion porosimetry of sintered TiO_2 scaffold from 60 ppi foam.

size of the original struts; (3) pores with a diameter of 385–700 μm and 310–385 μm, respectively. These regions correspond to the window size, the macroscopic distinguishable pores. These pores should be used as channels for the metabolism products. The three different pore sizes could also be observed in the SEM. However, the small sized pores within the ceramic part was actually larger as measured within the porosimetry. The overall porosity was 74%.

3.3. Permeability

The permeability rate is dependent of the foam's density (Fig. 10). Forty-five ppi foams with their large pores have a very good permeability of values up to 39% and decrease slightly with increasing density. The 60 ppi foams show, however, a strong correlation between decreasing permeability against increasing density. The lowest value, 4%, was found for the sample with the highest density. Hence, the higher the density the lower the permeability rate.

The 60 ppi foams had also lower permeability values which can be explained by the pore size of these structures being smaller and increasing the resistance of the flow media. The tortuosity, which was measured in the mercury intrusion meter, was several factors higher for 60 ppi foams compared to 45 ppi and therefore also understate the lower permeability.

Permeability measurements ($n=4$) of the mercury intrusion meter revealed values of 50 mDarcy for 60 ppi foams and 153 mDarcy for 45 ppi calculated by Eq. (3), and verify the higher permeability for scaffolds which were made with 60 ppi foams.

3.4. Cell adhesion test

More cells can be found in the 60 ppi foams compared to the 45 ppi foams. It can be explained by the simple fact that the macroscopic pore sizes of the 45 ppi foams are larger and cells simply fall through the foam's structure during the seeding. However, the cells have more space in the 45 ppi foams to spread themselves and to adhere onto the ceramic surface. The cells build a wide meshed network. Adhered cells are located into half open pores of the ceramic carrier. Also here, they are packed too closely to allow adherence at the ceramic surface.

Several cells adhere and circumstantially cover a single scaffold's strut (Fig. 11). A single fibroblast on the TiO_2 surface can be seen in (Fig. 12). These two SEM images are presented to show that fibroblasts adhere and feel well on the TiO_2 surface and that this cell adhesion is not specific to a designated area of the scaffold as the attachment covers the whole surface of the scaffold's structure.

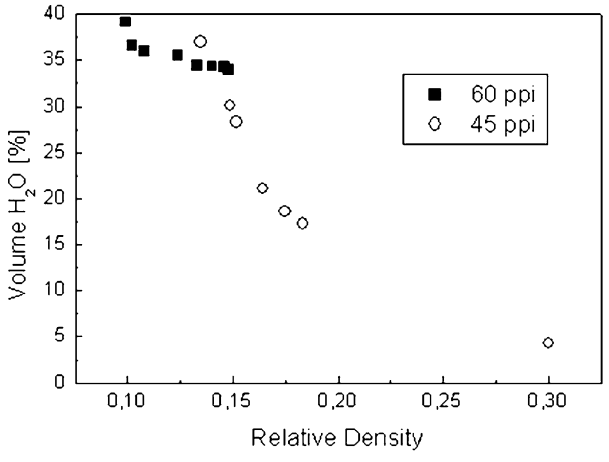

Fig. 10. Permeability of ceramic foams as a function of relative density. The flow rate through the "permeability meter" without a sample is taken as 100% ($n=10$).

4. Discussion and summary

The material's structural parameters not only control the cellular adhesion properties, but have been shown to

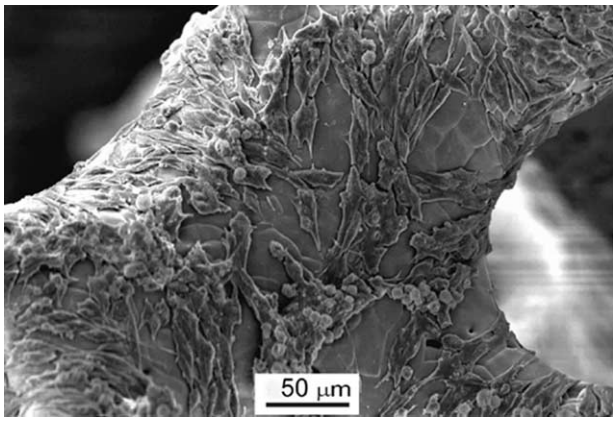

Fig. 11. Fibroblasts adhere and circumstantially cover a scaffold's strut of the TiO_2 surface.

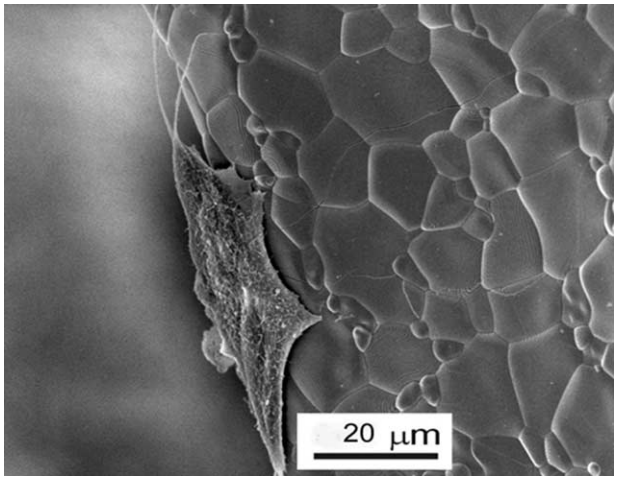

Fig. 12. A single fibroblast attached onto the TiO_2 scaffold surface.

directly affect viability, ingrowth, distribution and the formation of an ECM (Extracellular Matrix). The optimum pore size is different depending on cell types and its origin.[38] Hence, the ability to control the scaffold microarchitecture is of major importance.

Many natural and synthetic polymers, such as collagen, poly (α-hydroxyesters), poly (L-lactic acid)PLLA and poly(glycolic acid) PGA have been used due to the versatility and ease of processing for scaffold purposes.[31] However, some of their fabrication methods have limitations to their three-dimensional structure. E.g. solvent-casting/particulate leaching method[16] can only produce thin films of homogenous pore structure.[8] Gas foaming[7] generates defined microarchitecture, but encountered some problems in obtaining interconnective pores.[19]

It has been proven that a reproducible ceramic scaffold processing method has been established, where the three-dimensional structure can easily be adjusted in order to meet requirements for different cell culture seeding. The pore size is determined through the pore diameter of the polyurethane foam, where 60 ppi gave a median of 445 and 347 μm for the 45 ppi foams. The diameter of these foams before coating with a ceramic slurry was 1.7 and 1.1 mm, respectively. By using different foams of other ppi-numbers, the pore diameter can thus easily be adjusted. In order to achieve reproducible scaffolds, the density has to be kept constant.

The produced pores in the TiO_2 scaffolds were proven to be open and interconnective by permeability measurements. The permeability decreases with increasing density which can be explained simply by the fact that more ceramic slurry is present and decreases the pore diameter. The experimental data from the mercury intrusion porosimetry confirms the measurement from the permeability tester that the scaffolds with larger pore size diameters has a higher permeability rate, and that increased density lowers the permeability rate.

Mercury intrusion porosimetry shows three different pore size peaks (Fig. 9). These three different pore sizes could be observed in the SEM. However, the small sized pores within the ceramic part were actually larger as measured within the porosimetry. Error may be due to a higher inner pore diameter than the entrance diameter. The mercury fills these cavities and converts the intrusion volume to the distribution, and thus falsely represents the number of small pores. Hence the pores size distribution should be shifted more the larger pores, and the presence of smaller pores should be lower as observed in scanning electron microscope.

The scaffold structure seems to be very qualified for scaffold purposes as the fibroblast cells adhere onto its entire surface area. However some biological tests like vitality and mechanical tests are still missing, but the results of the initial cell culture tests are very promising. Some cells on the scaffold were dead (Fig. 11) and one reason may be that the growing medium and metabolism products can not easily be exchanged.

Several scaffold processing methods; phase-separation[13] and solvent-casting/particulate leaching,[16] require organic solvents. These residues may be remaining in these materials after processing, and hence may damage the seeded cells.[7] The scaffold fabrication of TiO_2 is free from any organic solvents due to the processing temperature.

There does not yet exist a scaffold mass production method of biocompatible materials. The fabrication methods which do exist are time-consuming, costly and often of low reproducibility.[8,30] As the ''polymer sponge method'' is already a known industrial manufacturing processing for open-cell ceramics, it is hoped, with the method described, to establish a mass production procedure of reproducible TiO_2 scaffolds with a defined macro- and microarchitecture.

References

1. Administration, H. R. A. S., Annual report of the US scientific registry for organ transplantation and the organ procurement and transplant network. The Division of Organ Transplantation. 1990.
2. Banavar, J. and Johnson, D., Characteristic pore sizes and transport in porous media. *Physical Review, Series B*, 1987, **35**, 7283–7286.
3. Boyan, B. D., Lohmann, C. H., Romero, J. and Schwartz, Z., Bone and cartilage tissue engineering. *Clinical Plastic Surgery*, 1999, **26**(4), 629–645, ix.
4. Drache, August 2002, Keramische Schaumfilter. Available at: http://www.drache-gmbh.de/eng/produkte.htm, Drache Umwelttechnik GmbH, D-65574 Diez. Online.
5. Garboczi, E. J., Mercury porosimetry and effective networks for permeability calculations in porous materials. *Powder Technology*, 1991, **6**(2), 121–125.
6. Gibson, L. J. and Ashby, M. F., Cellular solids—structure and properties. In, 2. Auflage ed. Cambridge University Press, Cambridge. 1997, pp. 205
7. Harris, L. D., Kim, B. S. and Mooney, D. J., Open pore biodegradable matrices formed with gas foaming. *Journal of Biomedical Material Research*, 1998, **42**(3), 396–402.
8. Hutmacher, D. W., Scaffold design and fabrication technologies for engineering tissues—state of the art and future perspectives. *Journal of Biomaterial Science Polymer Edition*, 2001, **12**(1), 107–124.
9. Jerome, R. and Maquet, V., Design of Macroporous Biodegradable Polymer Scaffolds for Cell Transplantation. *Materials Science Forum*, 1997, **250**, 15–42.
10. Jokinen, M., Pätsi, M., Rahiala, H., Peltola, T., Ritala, M. and Rosenholm, J. B., Influence of sol and surface properties on in vitro bioactivity of sol-gel-derived TiO_2 and TiO_2–SiO_2 films deposited by dip-coating method. *Journal of Biomedical Materials Research*, 1998, **42**(2), 295–302.
11. Katz, A. J. and Thompson, A. H., Prediction of rock electrical-conductivity from mercury injection measurements. *Journal of Geophysic Research—Solid Earth and Planets*, 1987, **92**, 599.
12. Katz, A. J. and Thompson, A. H., Quantitative prediction of permeability in porous rock. *Physical Review, Series B*, 1986, **34**(11), 8179–8181.
13. Lo, H., Ponticiello, M. S. and Leong, K. W., Fabrication of controlled release biodegradable foams by phase separation. *Tissue Engineering*, 1995, **1**, 15–28.

14. Luyten, J., Cooymans, J., De Wilde, A. and Thijs, I., Porous materials, synthesis and characterization. *Key Engineering Materials*, 2002, **206–213**(2), 1937–1940.
15. Mikos, A. G. and Temenoff, J. S., Formation of highly porous biodegradable scaffolds for tissue engineering. *Electronic Journal of Biotechnology*, 2000, **3**(2), 1–7.
16. Mikos, A. G., Thorsen, A. J., Czerwonka, L. A., Bao, Y. and Langer, R., Preparation and characterization of poly(L-lactic acid) foams. *Polymer*, 1994, **35**, 1068–1077.
17. Minnear, W. P., Presented at the Forming Science and Technology for Ceramics, Cincinnati,1991.
18. Montanaro, L., Jorand, Y., Fantozzi, G. and Negro, A., Ceramic foams by powder processing. *Journal of the European Ceramic Society*, 1998, **18**(9), 1339–1350.
19. Nam, Y. S., Yoon, J. J. and Park, T. G., A novel fabrication method of macroporous biodegradable polymer scaffolds using gas foaming salt as a porogen additive. *Journal of Biomedical Material Research*, 2000, **53**(1), 1–7.
20. Nygren, H., Eriksson, C. and Lausmaa, J., Adhesion and activation of platelets and polymorphonuclear granulocyte cells at TiO2 surfaces. *The Journal of Laboratory and Clinical Medicine*, 1997, **129**(1), 35–46.
21. Nygren, H., Tengvall, P. and Lundstrom, I., The initial reactions of TiO2 with blood. *Journal of Biomedical Materials Research*, 1997, **34**(4), 487–492.
22. Peng, H. X., Fan, Z., Evans, J. R. G. and Busfield, J. J. C., Microstructure of Ceramic Foams. *Journal of the European Ceramic Society*, 2000, **20**(7), 807–813.
23. Peters, M. C. and Mooney, D. J., Synthetic Extracellular Matrices for Cell Transplantation. *Materials Science Forum*, 1997, **250**, 43–52.
24. Piskin, E., Biomaterials in Different Forms for Tissue Engineering: An Overview. *Materials Science Forum*, 1997, **250**, 1–14.
25. Polonchuk, L., Elbel, J. L. E. J.B., Wintermantel, E. and Eppenberger, H. M., Titanium dioxide ceramics control the differentiated phenotype of cardiac muscle cells in culture. *Biomaterials*, 2000, **21**(6), 539–550.
26. Powell, S. J. and Evans, J., The structure of ceramic foams prepared from polyurethane ceramic suspensions. *Materials and Manufacturing Processes*, 1995, **10**(4), 757–771.
27. Saggio-Woyanski, J., Scott, C. E. and Minnear, W. P., Processing of porous ceramics. *American Ceramic Society Bulletin*, 1992, **71**(11), 1674–1682.
28. Schwartzwalder, K., and Somers, A. V., Method of Making a Porous Shape of Sintered Refractory Ceramic Articles. United States Patent No. 3090094, 1963.
29. Thomson, R. C., Shung, A. K., Yaszemski, M. J. and Mikos, A. G., Polymer Scaffold Processing. In *The principles of tissue engineering, Second ed*, ed. R. P. Lanza, R. Langer and J. Vacanti. Academic Press, San Diego, USA, 2000, pp. 251–261.
30. Thomson, R. C., Shung, A. K., Yaszemski, M. J. and Mikos, A. G., Polymer Scaffold Processing. In *Principles of Tissue Engineering*, ed. R. P. Lanza and R. Langer *et al*.. Academic Press, Austin, TX, 1997, pp. 251–261.
31. Thomson, R. C., Yaszemski, M. J., Powers, J. M. and Mikos, A. G., Hydroxyapatite fiber reinforced poly([alpha]-hydroxy ester) foams for bone regeneration. *Biomaterials*, 1998, **19**(21), 1935–1943.
32. Tomandl, G., and Müller, E., 2002, posting date. Allgemeine Information. Avaialble at: www.ww.tu-freiberg.de/lw/hauptseite.html, Institut für keramische Werkstoffe, D-09596 Freiberg.
33. Vacanti, J. and Vacanti, C., The challenge of tissue engineering. In *Principles of Tissue Engineering*, ed. R. P. Lanza and R. Langer *et al*.. Academic Press, Austin, TX, 1997, pp. 1–6.
34. Wake, M. C., Patrick, C. W. Jr. and Mikos, A. G., Pore morphology effects on the fibrovascular tissue growth in porous polymer substrates. *Cell Transplantation*, 1994, **3**(4), 339–343.
35. Whang, K., Healy, K. E., Elenz, D. R., Nam, E. K., Tsai, D. C., Thomas, C. H., Nuber, G. W., Glorieux, F. H., Travers, R. and Sprague, S. M., Engineering bone regeneration with bioabsorbable scaffolds with novel microarchitecture. *Tissue Engineering*, 1999, **5**(1), 5–51.
36. Wintermantel, E., Cima, L., Schloo, B. and Langer, R., Angiopolarity of cell carriers, Directional angiogenesis in resorbable liver cell transplantation devices. In *Angiogenesis: Principles-Science-Technology-Medicine*, ed. R. Steiner, B. Weisz and R. Langer. Birkhaeuser Verlag, Basel, 1992.
37. Wintermantel, E., Mayer, J., Ruffieux, K., Bruinink, A. and Eckert, K. L., Biomaterials, human tolerance and integration. *Der Chirurg*, 1999, **70**(8), 847–857.
38. Zeltinger, J., Sherwood, J. K., Graham, D. A., Mueller, R. and Griffith, L. G., Effect of pore size and void fraction on cellular adhesion, proliferation, and matrix deposition. *Tissue Engineering*, 2001, **7**(5), 557–572.